Electronic Supplementary Materials

For https://doi.org/10.1631/jzus.A2500232

Experience-guided optimization of jacket foundations for offshore wind turbines in varying water depths based on finite element analysis and the genetic algorithm

Jiajia HUANG[1,2], Tao JIN[1], Jianwu HUANG[1], Shasha SONG[3,4], Wei DAI[1], Chaoqun ZUO[1], Lizhong WANG[2], Lilin WANG[5], Zhen GUO[2]

[1]*China Energy Engineering Group Zhejiang Electric Power Design Institute Co., Ltd., Hangzhou 310012, China*
[2]*College of Civil Engineering and Architecture, Zhejiang University, Hangzhou 310058, China*
[3]*College of Civil Engineering, Tongji University, Shanghai 200092, China*
[4]*School of Civil Engineering, Shaoxing University, Shaoxing 312000, China*
[5]*Ocean College, Zhejiang University, Zhoushan 316021, China*

Section S1 Marine hydrographic conditions

Section S1.1 Design water level

The three representative engineering projects, referred to as Project A, Project B, and Project C, are located at offshore sites with varying water depths and environmental conditions. The corresponding water depths at these sites are 30.6 m, 60.23 m, and 89.81 m, respectively. According to hydrological observation data, the average water levels at the project sites are 0.30 m, 0.57 m, and 0.84 m, respectively, referenced to the National Elevation Datum of 1985. Based on a design return period of 50 years for OWT foundations, the calculated extreme high water levels are 4.47 m, 2.7 3m, 2.93 m, and the extreme low water levels are -3.84 m, -0.87m, -2.21m for the three projects. The design water levels for the three engineering projects are shown in Table S1.

Table S1 Design water levels for the three engineering projects

Return Period	Water Level Type	Project A	Project B	Project C
1 year	Mean water level (m)	0.30	0.57	0.44
	Design high water level (m)	3.27	1.58	2.36
	Design low water level (m)	-2.78	-0.57	-1.87
50 years	Extreme high water level (m)	4.47	2.73	2.93
	Extreme low water level (m)	-3.84	-0.87	-2.21

Section S1.2 Wind characteristics

Wind direction and wind speed levels were statistically analyzed by frequency, and the results were illustrated in the form of a wind rose diagram, as shown in Fig.S1. The wind conditions at the three offshore sites vary significantly in direction and speed, affecting jacket foundation design. Projects A and B, located in a subtropical monsoon climate, have consistent wind directions mainly from north-northeast and east-northeast, with frequencies of 40.9% and 49.2%. Most wind speeds at Project A (84.9%) are below 13.8 m/s, and at Project B (82.3%) below 12 m/s, indicating moderate winds. Project C shows more variable wind directions from northeast to south-southeast, with frequencies between 8.5% and 23.3%. The observed differences in dominant direction, speed

distribution, and directional variability highlight the necessity of site-specific design strategies for OWT foundations.

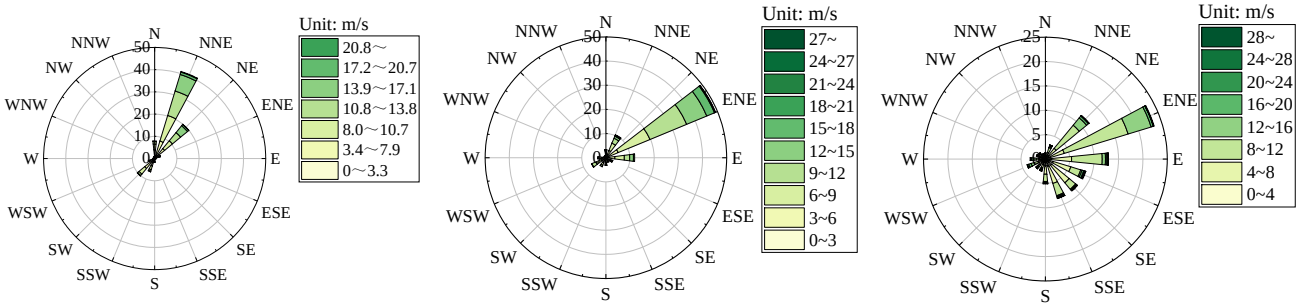

(a) Project A (b) Project B (c) Project C

Fig. S1 Wind rose diagrams of the three engineering projects, illustrating the frequency distribution of wind direction and significant wind speed.

Section S1.3 Wave characteristics

Wave characteristics play a critical role in determining the hydrodynamic forces and fatigue behavior of jacket foundations in offshore environments. Fig.S2 presents the wave rose diagrams for the three engineering projects. Project A experiences a moderately energetic wave climate dominated by east-northeast and northeast directions, with 76.4% of waves under 3.0 m but a relatively high proportion (7.7%) of wave events exceeding 5.0 m. Project B presents a more stable and moderate wave field, with waves from the east and directions close to east-northeast accounting for most occurrences. Here, 95.2% of waves below 3.0 m, and only 0.42% exceed 5.0 m. Project C shows the vast majority of waves are below 3m, accounting for 82.6%. Higher waves exceeding 5 m occur more frequently, representing about 8.7%. The directional spread of the wave is relatively broad at project C, predominantly ranging from east-northeast to southeast, which indicates a more distributed wave loading pattern. In contrast, Projects A and B demonstrate more concentrated wave directions.

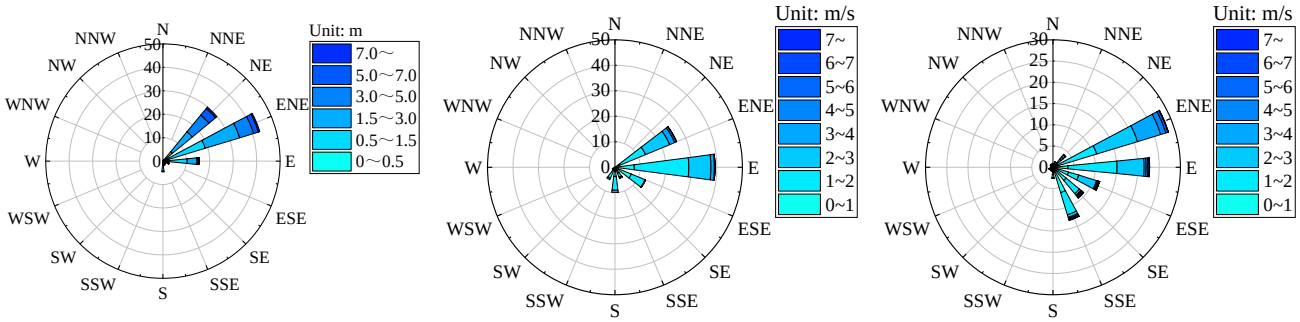

(a) Project A (b) Project B (c) Project C

Fig. S2 Wave rose diagrams of the three engineering projects, illustrating the frequency distribution of wave direction and significant wave height.

Section S1.4 Design values of wave and current

Design values of wave and current are critical for evaluating the structural response and safety of offshore foundations under both operational and extreme conditions. These parameters typically include wave height, wave period, and current velocity, each corresponding to specific return

periods (e.g., 1-year for operational design and 50-year for extreme conditions). Differences in water depth and regional oceanographic conditions result in significant variability across project sites. Table S2 summarizes the design values of wave and current parameters for Projects A (30.06 m), B (60.23 m), and C (89.81 m), based on 1-year and 50-year return periods. Under the 1-year return period, H_1% wave height (the wave height exceeded by only 1% of the total wave records during a given period) range from 6.12 m to 9.34 m, with associated mean wave periods (T□$_{ea}$□) between 8.06 s and 9.52 s. For extreme sea states corresponding to the 50-year return period, H_{max} wave (the largest vertical distance between a wave crest and the adjacent trough recorded within a given observation period.) heights increase notably, with values reaching up to 23.58 m at Project C, and wave periods extending to 14.63 s.

Table S2 Design values of wave and current parameters for the three Projects based on 1-year and 50-year return periods.

Type	Return Period	Design water level	Parameters	Project A (30.06m)	Project B (60.23m)	Project C (89.81m)
Wave	1 year	Design high water level	$H_{1\%}$ (m)	6.33	8.86	9.34
			T_{mean} (s)	8.06	8.62	9.46
		Design low water level	$H_{1\%}$ (m)	6.12	7.58	9.02
			T_{mean} (s)	8.11	8.67	9.52
	50 years	Extreme high water level	H_{max} (m)	18.87	20.34	23.58
			T_{mean} (s)	12.46	13.32	14.63
		Extreme low water level	H_{max} (m)	17.05	18.56	21.70
			T_{mean} (s)	11.96	12.79	14.05
Current	1 year	Surface current velocity (m/s)		2.25	1.96	1.82
		Bottom current velocity (m/s)		2.05	1.35	0.95
	50 years	Surface current velocity (m/s)		2.63	2.46	2.37
		Bottom current velocity (m/s)		2.37	1.57	1.23

In terms of current conditions, surface and bottom current velocities are provided for both return periods. For the 1-year condition, surface current velocities range from 1.82 m/s to 2.25 m/s, and bottom current velocities range from 0.95 m/s to 2.05 m/s. Under the 50-year return condition, maximum surface current velocities reach 2.63 m/s at Project A, while bottom current velocities are below 2.4 m/s across all sites. These design values reflect the variation in hydrodynamic intensity with water depth, and provide the basis for structural load assessments and safety verification of offshore foundations under operational and extreme conditions.

Section S2 Description of the finite element model for the jacket foundation

Section S2.1 Structural configuration

Based on the marine hydrodynamic and geotechnical conditions of the three representative offshore engineering projects, a jacket foundation model for OWTs was developed using the offshore structural analysis software SACS. Fig.S3 presents the schematic diagram of the jacket foundation. The upper jacket structure consists of four double-inclined main legs and multiple levels of diagonal bracing members, all fabricated from circular steel tubular sections. The bracing system adopts an “X-type” configuration. The top of the vertical main steel tubular members is connected to the wind turbine tower via a transition piece, which transfers the turbine loads from

the tower to the jacket foundation. Meanwhile, the jacket also withstands environmental loads such as wind, wave, and current forces, which are further transmitted to the pile foundation through grouted connection segments. The pile foundation consists of four steel tubular piles arranged uniformly in a square configuration, with a 5-meter allowance reserved for potential scour depth. To prevent local buckling failure at the pile head and tip during installation, as well as stress concentration failure in the grouted segment near the pile top, localized thickening is applied at the pile head and tip. Both the upper jacket and the piles are made of DH36 structural steel, with a yield strength of no less than 355 MPa and a tensile strength ranging from 490 to 630 MPa. In this study, the yield strength is taken as 355 MPa and the tensile strength as 490 MPa. In addition, as illustrated in Fig. S3, the transition piece is modelled together with the jacket structure and pile foundation in SACS to preserve the overall geometric continuity of the support structure, but it is excluded from the finite element analysis in this study and is not considered within the following GA optimization framework.

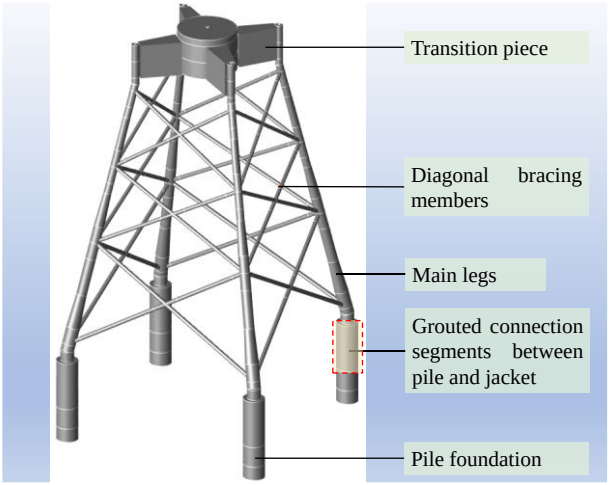

Fig. S3. Schematic diagram of the jacket foundation for OWT.

Section S2.2 Design load analysis

In the design of OWT foundations, load cases are typically categorized into ultimate limit state (ULS), serviceability limit state (SLS), accidental limit state (ALS, such as rare seismic events), and fatigue limit state (FLS). Among these, the ULS and FLS conditions are often the governing cases. To improve computational efficiency, only ULS and FLS load cases are considered in this study. For the ULS, environmental loads—including wind, wave, and current—are applied using a quasi-static approach following the recommendations of API RP 2A-WSD (API, 2019) for fixed offshore structures. Extreme design load cases are defined based on API-specified environmental load combinations, and the corresponding static equivalent loads are used in the finite element analysis. For the FLS, long-term load histories are transformed into equivalent fatigue loads representing the full-life fatigue effect on the jacket foundation, in accordance with API RP 2A-WSD and DNV-RP-C203 (DNV, 2016). These equivalent fatigue loads serve as input for finite element fatigue analysis to assess the service life of critical joints. The primary load categories considered include:

(1) Structural self-weight (F_{weig}), including the weight of the foundation structure and its attached components, and marine growth attached to the structure, with buoyancy effects duly considered. The marine growth thickness is set at 100 mm from the scour surface to the design high water level and the dry density is taken as 1.35×10^{3} kg/m^{3}. The foundation buoyancy calculation considers the watertight properties of structural members. For watertight members, buoyancy is

computed based on their full volume, while for permeable members, it is based on the effective displaced water volume.

(2) Wind turbine loads (F_{turb}), referring to the loads transmitted to the base of the tower from the upper structure (including the wind turbine and tower) induced by wind action, self-weight, and other operational effects. The rotor–nacelle assembly (RNA) is represented in the finite element model using lumped parameters rather than explicit blade modelling. A 16.7 MW offshore wind turbine is employed in this study, with the load parameters provided in Table S3. The RNA's lumped properties—including total mass, center of gravity, and moments of inertia—are defined in the tower-top coordinate system, as listed in Table S4, to capture the inertial characteristics of the RNA in the structural analysis. The tower is modelled as a conical steel structure with a base diameter of 8.2 m tapering to 6.1 m at the top, wall thickness decreasing from 45 mm at the base to 22 mm at the top, and an overall height of 121.5 m.

Table S3 Load parameters of the OWT

Load cases	Horizeontal load F_{xy} (kN)	Vertical load F_z (kN)	Bending moment M_{xy} (kNm)	Torque M_z (kNm)
ULS	2793	-11793	280181	-3726
FLS	791	306	81895	17821

Table S4 The lumped parameters of the RNA in the tower top coordinate system

coordinate axis	Mass (t)	Center of gravity (m)	Moment of inertia (10^8 kgm^2)
X-axis		-2.264	3.75
Y-axis	643.1	0.031	2.14
Z-axis		2.861	2.17

(3) Wave loads (F_{wave}). The wave load is calculated based on the Morison's equations according to DNV-OS-J101(DNV, 2014) and the Morison's equations compose of an inertia and a drag term and can be written as follows,

$$F_{wave} = \frac{1}{4}\pi\rho_w D^2 C_M \frac{du}{dt} + \frac{1}{2}\rho_w D C_D u|u| \quad \text{(S1)}$$

where ρ_w is the density of water, with typical value of 1028 kg/m^3; D is the member diameter; C_M and C_D are the inertia and drag coefficients of the member, according to API RP 2A-WSD (2019), C_M is taken as 1.6 for smooth members and 1.2 for rough members, C_D is taken as 0.65 for smooth members and 1.05 for rough members; t is time; $u(t)$ is horizontal velocity of water particles, which are calculated based on stream function wave theory (Dean, 1965).

(4) Current loads (F_{curr}). Current can induce drag loads on the support structure. The current load is calculated using the combined wave–current coupling method, in which the current velocity is superimposed to the wave velocity in the drag term of the Morison's equation in Eq.(S1). (Chakrabarti, 1987; DNV 2019). As the current velocity is generally steady (i.e. with negligible acceleration), it does not contribute to the inertia term.

Section S2.3 Design Load Cases

Since structural optimization involves extensive computational iterations, only the potentially governing conditions—namely, the ULS and FLS—are considered during the iterative optimization

process to improve computational efficiency.

Section S2.3.1 ULS case

The environmental design parameters are based on a 50-year return period in ULS case. The computational model was developed in accordance with industry standards API RP 2A-WSD (API, 2019) and DNV-RP-C205 (DNV, 2019), incorporating systematic load modeling and combination schemes for wind turbine loads, wave actions, ocean currents, and structural self-weight. The structural loading calculations consider both perpendicular (0°) and diagonal (45°) loading directions (shown in Fig.S4) to determine the most critical combinations of wind turbine and environmental loads under ULS conditions. Environmental loads on the jacket structure were simulated under combinations of wave and current actions corresponding to different design water levels—namely, extreme high water level, extreme low water level, design high water level, and design low water level. A full-circle wave loading analysis was conducted with a wave step size of 5°, producing 72 discrete wave directions ranging from 0° to 355°. The current field was defined using a layered velocity profile to reflect the varying flow speeds between the near-bed and surface layers. Each wave direction corresponds to a static load case, enabling the model to comprehensively capture the directional variability of wave-induced forces.

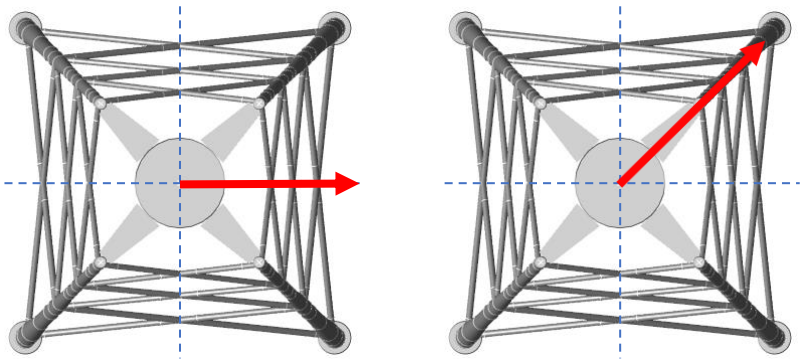

(a) 0° (b) 45°

Fig. S4. Load directions in the computational analysis of the jacket foundation.

A total of 16 representative load combinations in ULS case were established. Each load combination includes three main components: (1) Wind turbine loads (F_{turb}), applied in 0° and 45° directions (WT00, WT45), respectively; (2) Wave and current loads (F_{wave}+F_{curr}), the two wave loading scenarios were considered under identical water level conditions: maximum overturning moment and maximum base shear (EM00, EM45, ES00, ES45). Each case captures the critical structural response by optimizing the wave position to produce either the maximum overturning moment or the maximum base shear; (3) Structural self-weight (F_{weig}), incorporating the dead weight of the platform and associated facilities. A detailed summary of the load combinations is presented in Table S5. According to DNV code DNV-OS-J101(DNV, 2014) and Chinese code GB 50009-2012 (2012), the load combination with the worst-case ultimate response is defined as $1.35\times F_{turb}+1.35\times 0.7\times(F_{wave}+F_{curr})+1.1\times F_{weig}$ for the compressive capacity check, and $1.35\times F_{turb}+1.35\times 0.7\times(F_{wave}+F_{curr})+0.9\times F_{weig}$ for the uplift capacity check. These combinations were designed to maximize structural response under each scenario, ensuring the representativeness and conservatism of the load cases.

In the ULS case, the framework computes critical structural performance indicators such as axial compressive and uplift capacities, along with unity check (UC) values for members, joints, and pile shaft stresses, based on combined loading scenarios. Modal analysis is also integrated to determine the natural frequencies and mode shapes of the jacket foundation, which are essential for preventing resonance with wave and wind turbine excitation.

Table S5 Definition of load combinations for ULS analysis

Load Combination Case ID	Design water level	Directions	Wind turbine loads	Environmental loads	Structural self-weight
LCM1	Extreme high water level	0 °	WT00	EM00	SW
LCM2			WT00	ES00	
LCM3		45 °	WT45	EM45	
LCM4			WT45	ES45	
LCM5	Extreme low water level	0 °	WT00	EM00	
LCM6			WT00	ES00	
LCM7		45 °	WT45	EM45	
LCM8			WT45	ES45	
LCM9	Design high water level	0 °	WT00	EM00	
LCM10			WT00	ES00	
LCM11		45 °	WT45	EM45	
LCM12			WT45	ES45	
LCM13	Design low water level	0 °	WT00	EM00	
LCM14			WT00	ES00	
LCM15		45 °	WT45	EM45	
LCM16			WT45	ES45	

Section S3.3.2 FLS case

Fatigue assessment is a critical component in the design of OWT jacket foundations, particularly due to the long operational lifespan and continuous exposure to cyclic environmental loads. FLS analysis is conducted to evaluate the cumulative damage induced by load-induced stress variations over time. The computation is based on long-term environmental statistics, with wave scatter data used to simulate representative sea states. The fatigue analysis was performed based on the S–N curves and Miner linear cumulative damage rule, considering the combined effects of wind turbine loading and wave loading. Under wind turbine loading, a deterministic fatigue analysis was conducted using the equivalent fatigue loads of the turbine. For wave loading, spectral fatigue analysis was carried out based on the wave scatter diagram. According to DNV-RP-C203 (DNV, 2016), the mathematical representation of the S–N curve for fatigue analysis is given as follows:

$$\log_{10}(N) = \log_{10}(a) - m\log_{10}\left(\Delta\sigma\left(t_c / t_{ref}\right)^k\right) \quad \text{(S2)}$$

where N is fatigue life, defined as the number of cycles to failure under a stress range $\Delta\sigma$ (MPa); $\log_{10}(a)$ is the intercept on the $\log_{10}(N)$ axis; m is the negative tangent slope of the S–N curve; t_{ref} is the reference wall thickness, it is set to be 32 mm for tubular joints, while for other types of joints, such as circumferential welds, it is 25 mm; t_c is the thickness along which a crack may propagate; k is the thickness exponent.

The fatigue life of the foundation is evaluated using Miner cumulative damage rule. According to Miner linear cumulative damage theory, the damage incurred under a stress level S_i after n_i cycle

is given by $D_i=n_i/N_i$, in which N_i is the fatigue life under the stress level S_i. If the structure experiences n_i cycle at M different stress levels S_i, the total damage can be defined as:

$$D_C = DEF\sum_{i=1}^{I}\frac{n_{C,i}}{N_{C,j}} \le 1.0 \tag{S3}$$

where D_C is the characteristic cumulative fatigue damage; $n_{C,j}$ is the number of stress cycles in the i-th segment obtained from the characteristic long-term stress range distribution; $n_{C,j}$ is the number of failure cycles for the i-th segment obtained from the characteristic S–N curve; DEF is the design fatigue factor, taken as 3.0 for wind turbine foundations.

Fatigue analysis is conducted based on the turbine fatigue load spectra and wave spectra, taking into account different loading weight coefficient associated with various wind and wave directions. The total structural fatigue damage is then determined by linearly accumulating the damage contributions from each loading scenario.

Section S2.4 Nonlinear pile-soil interaction and pile capacity

The jacket foundation comprises steel tubular driven piles that serve to transmit the applied loads into the supporting seabed. To capture the nonlinear behavior of the soil–pile interface under cyclic and static loading, a series of load-transfer curves were developed in API RP 2A-WSD (API, 2019) and API RP 2GEO (API, 2014): (1) The *p*-*y* curve, describing the lateral soil reaction per unit pile length as a function of lateral deflection. For soft clay, the Matlock (1970) model was used, while for sand, Reese *et al.* (1974) formulations were adopted. (2) The *t*–z_f curve, which characterizes the relationship between axial shaft friction and pile displacement, is developed based on API-specified limiting skin friction and empirical models derived from field observations. (3) The *Q*–z_p curve, characterizing the relationship between the end-bearing capacity and the displacement at the pile tip, was defined through hyperbolic models correlating axial tip settlement to end-bearing resistance. These nonlinear load–displacement curves were discretized and applied as spring elements in the pile-soil interaction modeling, where lateral springs (*p*–*y*) were distributed along the pile shaft to simulate soil lateral confinement, and vertical axial springs (*t*-z_f and *Q*–z_p) were assigned to represent shaft and tip resistance. The springs operate under one-directional nonlinear constitutive laws with user-defined stiffness degradation, allowing accurate simulation of staged and cyclic loading. Soil layering and depth-dependent parameters were taken into account based on geotechnical site investigation data. According to the stratigraphic data presented in Table S6, the three types of nonlinear pile-soil interaction curves under a preliminary design scheme (with a pile penetration depth of 85 m and a pile diameter of 3.0 m) can be obtained, as shown in Fig.S5.

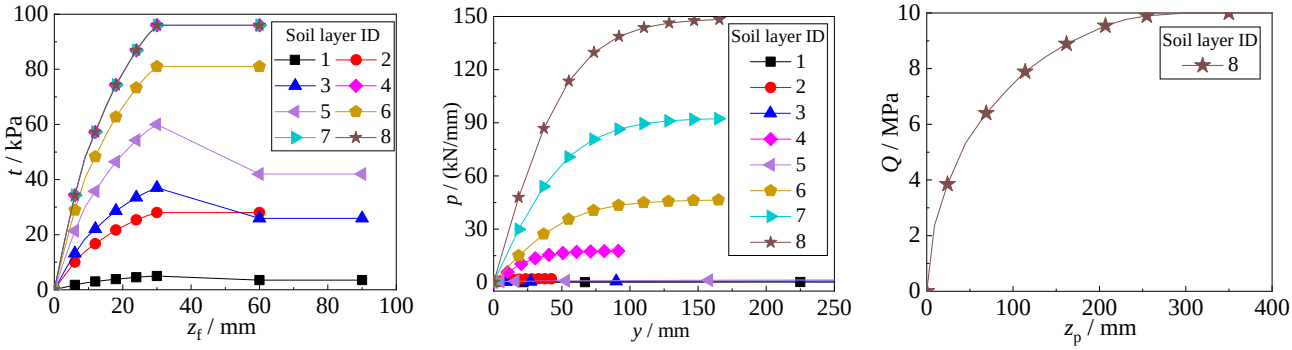

(a) *t*-z_f curve (b) *p*-*y* curve (c) *Q*-z_p curve

Fig.S5 Nonlinear pile–soil interaction curves for a pile 85 m long and 3 m in diameter.

The ultimate axial capacity of piles in compression Q_c consists of the shaft friction capacity $Q_{f,c}$ and the end bearing capacity Q_p, can be determined by the equation according to API RP 2GEO (API, 2014):

$$Q_C = Q_{f,c} + Q_p = f(z)A_s + qA_p \tag{S4}$$

where $f(z)$ is the unit shaft friction, kPa; A_s is the side surface area of pile, m^2; q is the unit end bearing at the pile tip, kPa; A_p is the gross end area of the pile, m^2; z is the depth below the original seafloor, m.

For pipe piles in cohesive soils, the unit shaft friction $f(z)$ at depth z, can be calculated using Eq.(S5)

$$f(z) = \alpha s_u \tag{S5}$$

where s_u is the undrained shear strength of the soil at the point z, kPa; α is the dimensionless shaft friction factor for clays, $\alpha=0.5\psi^{-0.5}$ for $\psi\leq1.0$ or $\alpha=0.5\psi^{-0.25}$ for $\psi>1.0$ with the constraint that $\alpha\leq1.0$, in which $\psi=s_u/p'_o(z)$, $p'_o(z)$ is effective vertical stress at depth z, kPa. The unit end bearing q for cohesive soils can be computed using $q=9s_u$.

For pipe piles in cohesionless soils, the unit shaft friction $f(z)$ at a given depth z, can be calculated by Eq.(S6) (API, 2014).

$$f(z) = Kp'_o(z)\tan\delta \tag{S6}$$

where K is the dimensionless lateral earth pressure coefficient, defined as the ratio of horizontal to vertical effective stress; δ is the interface friction angle between pile and soil. The unit end bearing q for cohesionless soils can be computed using $q=N_q p'_o(z)$, in which N_q is the dimensionless bearing capacity factor. Additionally, the API specification stipulates that the pile axial capacity in tension Q_t shall not exceed the total shaft friction $Q_{f,c}$ in compression. Nevertheless, no explicit analytical expression is provided for calculating this limitation in API specifications. Therefore, the pile axial capacity in tension Q_t in this study is defined as $Q_t=\xi Q_{f,c}+G_p$ (JTS 167-2018), in which ξ and G_p are the uplift reduction coefficient presented in Table S6 and the weight of the pile, respectively.

Section S3 Design Constraints

U_{mem} is taken as the maximum of $U_{mem,NM}$ and $U_{mem,TV}$, that is,

$$U_{mem} = \max\left(U_{mem,NM}, U_{mem,TV}\right) \tag{S7}$$

where $U_{mem,NM}$ ($U_{mem,TV}$) is the UC value of the member subjected to combined axial and bending (beam shear and torsional shear) forces, and the two UC values are expressed as:

$$U_{mem,NM} = \frac{\gamma_R \sigma_m}{f_y} + \frac{\gamma_{R,b}\sqrt{\sigma_{b,y}{}^2 + \sigma_{b,z}{}^2}}{f_b} \tag{S8}$$

$$U_{mem,TV} = \frac{\tau_b}{f_{v,t}/\gamma_R} \tag{S9}$$

where γ_R is the partial resistance factor; σ_m is the axial stress of the member due to forces; f_y is the representative yield strength; $\gamma_{R,b}$ is the partial resistance factor for bending strength; $\sigma_{b,y}$ or $\sigma_{b,z}$ is the bending stress about the member y-axis (in-plane) or z-axis (out-of-plane) due to forces; f_b is the representative bending strength; τ_b is the maximum shear stress due to forces; $f_{v,t}$ is the representative shear strength of the member subjected to combined beam shear forces and torsional shear forces.

The load UC of joint U_{jold} can be written as:

$$U_{\text{josr}} = \left|\frac{P_{\text{B}}}{P_{\text{d}}}\right| + \left(\frac{M_{\text{B}}}{M_{\text{d}}}\right)^2_{\text{ipd}} + \left|\frac{M_{\text{B}}}{M_{\text{d}}}\right|_{\text{opd}} \tag{S10}$$

where P_{B} or M_{B} is the axial force or bending moment in the brace; P_{d} or M_{d} is the design value of the joint axial strength or bending moment strength; ipb or opb represents in-plane or out-of-plane bending. For the joint strength UC, as specified in API RP 2A-LRFD, the chord cans must have a minimum axial capacity of at least 50 % of the effective strength of each incoming brace under all relevant design conditions. The strength UC reflects the inherent strength characteristics of the joint configuration, independent of its actual in-service load history, thereby enabling consistent evaluation and comparison of reserve capacities across different joint geometries and design scenarios. The shaft stress UC value of a pile U_{pile} evaluates the ratio of the combined axial and bending stresses in a pile segment to the corresponding allowable stresses, and can thereby be calculated according to Eq.(S12).

Table S6 Physical and mechanical properties of the main geotechnical layers

Soil layer ID	Soil type	Bottom Depth of Layer h (m)	Natural Unit Weight γ (kN/m^3)	Undrained Shear Strength s_u(kPa)	Strain at Half of Peak Principal Stress ε_{50}	Internal Friction Angle φ	Bearing Capacity Factor N_q	Uplift Reduction Coefficient ξ
1	Mud	8.8	16	10	0.03	/	/	0.6
2	Silt	19.1	19	/	/	32	28	0.6
3	silty clay	26.1	18.1	40	0.012	/	/	0.7
4	Fine Sand	36.8	19.5	/	/	35	40	0.6
5	silty clay	52.4	19	60	0.007	/	/	0.7
6	Silty Fine Sand	53.9	19.8	/	/	33	40	0.6
7	Fine to Medium Sand	63.1	20	/	/	36	40	0.6
8	Fine to Medium Sand	100	20.2	/	/	37	40	0.6

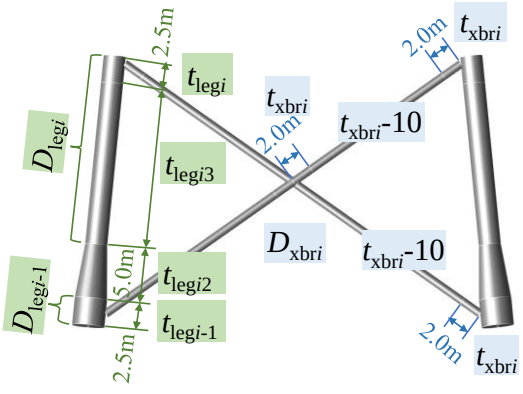

$$D_{\text{leg}i} = \begin{cases} D_{\text{leg0}} = x_3 & (i=0) \\ D_{\text{leg0}} - \Delta D_{\text{leg}i,0} = x_3 - x_{i+3} & (i=1,2,3,4,5) \end{cases}$$

$$t_{\text{leg}i} = \begin{cases} t_{\text{leg0}} = x_9 & (i=1) \\ t_{\text{leg0}} - \Delta t_{\text{leg}i,0} = x_9 - x_{i+9} & (i=1,2,3,4,5) \end{cases}$$

$$D_{\text{xbr}i} = \begin{cases} D_{\text{xbr1}} = x_{15}, & (i=1) \\ D_{\text{xbr1}} - \Delta D_{\text{xbr}i,1} = x_{15} - x_{i+14}, & (i=2,3,4,5) \end{cases}$$

$$t_{\text{xbr}i} = \begin{cases} t_{\text{xbr1}} = x_{20}, & (i=1) \\ t_{\text{xbr1}} - \Delta t_{\text{xbr}i,1} = x_{20} - x_{i+19}, & (i=2,3,4,5) \end{cases}$$

Fig.S6 Schematic diagram of a typical jacket layer and associated optimization design variables

Table S7 The optimization design variables for the three projects

Design variables group	Design variables						
	Project A (30.06m)	Project B (60.23m)	Project C (89.81m)	step size	lower bound	upper bound	Remarks
Top and bottom leg spacings	x_1	x_1	x_1	0.1 m	100	200	Top leg spacing L_{top}
	x_2	x_2	x_2	0.01	120	300	the ratio of bottom leg spacing to bottom leg spacing
Diameter of the main leg	x_3	x_3	x_3	10 mm	150	350	the diameter of the bottom main leg D_{leg0}
	x_4	x_4	x_4		0	150	the difference of D_{leg0} to D_{legi}, i.e. D_{leg0}- D_{legi}
	x_5	x_5	x_5		0	150	
	x_6	x_6	x_6		0	150	
		x_7	x_7		0	150	
			x_8		0	150	
Wall thickness of the main leg	x_7	x_8	x_9	1 mm	40	100	the wall thickness of the bottom main leg t_{leg0}
	x_8	x_9	x_{10}		-10	50	the difference of t_{leg0} to t_{legi}, i.e. t_{leg0}- t_{legi}
	x_9	x_{10}	x_{11}		-10	50	
	x_{10}	x_{11}	x_{12}		-10	50	
		x_{12}	x_{13}		-10	50	
			x_{14}		-10	50	
Diameter of the diagonal bracing members	x_{11}	x_{13}	x_{15}	10 mm	50	150	The diameter of the bottom diagonal bracing member D_{xbr1}
	x_{12}	x_{14}	x_{16}		-10	30	the difference of D_{xbr1} to D_{xbri}, i.e. D_{xbr1}-D_{xbri}
	x_{13}	x_{15}	x_{17}		-10	30	
		x_{16}	x_{18}		-10	30	
			x_{19}		-10	30	
Wall thickness of the diagonal bracing member	x_{14}	x_{17}	x_{20}	1 mm	30	60	The wall thickness of the bottom diagonal bracing member t_{xbr1}
	x_{15}	x_{18}	x_{21}		-10	30	the difference of t_{xbr0} to t_{xbri}, i.e. t_{xbr0}- t_{xbri}
	x_{16}	x_{19}	x_{22}		-10	30	
		x_{20}	x_{23}		-10	30	
			x_{24}		-10	30	
Pile-related parameters	x_{17}	x_{21}	x_{25}	0.1 m	400	800	The embedded depth L_{empl}
	x_{18}	x_{22}	x_{26}	10 mm	250	500	The diameter D_{pile}

	x_{19}	x_{23}	x_{27}	1 mm	40 mm	80 mm	The maximum wall thickness t_{p1}

References

[1] API (American Petroleum Institute), 2014. Geotechnical and Foundation Design Recommendations, API RP 2GEO. Washington, D.C., API Publishing.

[2] Chakrabarti, S.K., 1987. Hydrodynamics of offshore structures: Mathematical theory and its applications in structures. WIT Press.

[3] Dean, R.G., 1965. Stream function representation of nonlinear ocean waves. Journal of Geophysical Research, 70(18), 4561–4572. https://doi.org/10.1029/JZ070i018p04561

[4] DNV (Det Norske Veritas). 2014. Offshore standard for design of offshore wind turbine structures, DNV-OS-J101. Høvik, Norway, DNV.

[5] DNV (Det Norske Veritas). 2016. Fatigue design of offshore steel structures, DNV-RP-C203. Høvik, Norway, DNV.

[6] DNV (Det Norske Veritas). 2019. Environmental conditions and environmental loads, DNV-RP-C205. Høvik, Norway, DNV.

[7] Matlock, H., 1970. Correlation for design of laterally loaded piles in soft clay. The Offshore Technology Conference, Houston, Texas: OTC-1204-MS. https://doi.org/10.4043/1204-MS

[8] Ministry of Housing and Urban-Rural Development of the People's Republic of China, 2012. Load Code for the Design of Building Structures, GB 50009-2012. Beijing, China Architecture & Building Press. (in Chinese)

[9] Ministry of Transport of the People's Republic of China, 2018. Design Code for Wharf Structures, JTS 167-2018. Beijing, China Communication Press. (in Chinese)

[10] Reese, L.C., Cox, W.R., Koop, F.D., 1974. Analysis of laterally loaded piles in sand. The Offshore Technology Conference, Houston, Texas: OTC-2080-MS. https://doi.org/10.4043/2080-MS